The Long-Term Dynamical Behavior of Short-Period Comets

HAROLD F. LEVISON

Space Science Department, Southwest Research Institute, San Antonio, Texas 78238
E-mail: hal@gort.space.swri.edu

AND

MARTIN J. DUNCAN

Department of Physics, Queen's University, Kingston, Ontario, Canada K7L 3N6

We have developed and carefully tested a new computer code to follow the long-term dynamical evolution of a swarm of test particles in the solar system. This new integrator is approximately an order of magnitude faster than previously existing codes. The technique efficiently and accurately handles close approaches between test particles and planets while retaining the powerful features of recently developed mixed variable symplectic integrators.

We use the new code to numerically integrate the orbits of the known short-period comets (those with periods $P < 200$ years) under the influence of the Sun and all the planets except Mercury and Pluto, for times up to 10^7 years. It is found under a classification based on period that most comets move between Jupiter-family ($P < 20$ yr) and Halley-family ($P > 20$ yr) orbits many times in their dynamical lifetimes. However, it is found that the Tisserand parameter, T, does not vary substantially for most comets. Therefore, we adopt a classification originally suggested by Carusi *et al.* (1987) that defines Jupiter-family comets (JFCs) as comets with $T > 2$ and Halley-family comets (HFCs) as those with $T < 2$. In this scheme, less than 8% of comets change families during the integration and most of those that change tend to remain near the Tisserand dividing line throughout. Thus, the JFCs (as defined by the Tisserand parameter) are dynamically distinct from the HFCs. We find that in our forward integration, 92% of comets are ejected from the solar system, and that ≈6% are destroyed by becoming sun-grazers. The number of sun-grazers is far more than would be expected from the existing analytic theories. The median lifetime of all known short-period comets from the current time to ultimate destruction or ejection is approximately 4.5×10^5 years. The very flat inclination distribution of Jupiter-family comets is found to become more distended as it ages. Since JFCs are dynamically distinct from HFCs, they must have an inclination distribution, when they first become visible, that is even flatter than that currently observed. For reasonable values of the physical lifetime before fading, we calculate that there should be roughly 5–20 times as many extinct JFCs as currently known JFCs. Our prediction for the mean cos (i) of the extinct JFCs is consistent with the existing data on these objects. © 1994 Academic Press, Inc.

1. INTRODUCTION

Understanding the origin and evolution of comets is critical to understanding the origin of the solar system because comets are thought to be the remnants of the icy planetesimals that formed Uranus and Neptune, and to a lesser degree Jupiter and Saturn. Comets may have also been an important source of the volatiles on the Earth.

Short-period comets (those with periods P less than 200 years, hereafter SPCs) have been of particular interest recently because of a controversy in the literature concerning their origin. It had been widely believed that SPCs originated in the Oort cloud and evolved into SPC orbits through gravitational interactions with the planets (Newton 1893; see also Everhart 1972). However, in recent years several lines of argument have shown that it is not possible to reproduce the very flat inclination distribution of the majority of SPCs from a spherical Oort cloud.

Fernández (1980) was the first to suggest that Jupiter-family comets (which he defines as those with $P < 20$ years) originate in a disk of material that lies just beyond the orbit of Neptune. Duncan *et al.* (1988; see also Quinn *et al.* 1990, hereafter QTD) showed that many objects that are initially on low inclination orbits with semimajor axes near 50 AU evolve into orbits that are consistent with those of Jupiter-family comets. They therefore argued that this disk of comets is the source for the Jupiter family. Stagg and Bailey (1989) presented counterarguments to this idea. Levison (1991) argued that this controversy will not be solved until a better understanding of both the current state and the evolution of the complete short-period population becomes available.

The distribution of orbital elements of the complete population of SPCs is uncertain. The sample of short-period comets is affected by observational biases that tend

to select objects with small semimajor axes and perihelion distances and perhaps low inclinations (Kresák 1981; Shoemaker and Wolfe 1982). Several attempts have been made to correct for these biases (e.g., Shoemaker and Wolfe 1982; Fernández et al. 1992), but the distribution of the complete population remains poorly understood.

In addition, the long-term dynamical behavior of short-period comets is poorly understood and there are only rough estimates of their dynamical lifetimes. Öpik (1963) calculated the expected dynamical lifetimes of 16 SPCs using a statistical semianalytic theory. He found that the median lifetime for his sample is approximately 2.5×10^6 years. There have been many efforts to study the dynamical behavior of the short-period comets by direct numerical integration of their orbits (Kazimirchak-Polonskaya 1967; Belyaev 1967; Carusi et al. 1985; Nakamura and Yoshikawa 1991; and Tancredi and Rickman 1992). However, these integrations have been limited to timescales that are much less then the dynamical lifetimes of these objects, the longest previous integration being about 4000 years. Therefore, none of these integrations have been able to directly calculate the dynamical lifetimes of SPCs.

It is only with very recent developments in numerical techniques and advances in computer hardware that very long numerical integrations of comet orbits can be achieved.

In this paper we undertake an integration of the orbits of all 160 comets known in 1991 with current periods less than 200 years. The integration extends forward and backward in time for 10^7 years. We integrate four orbits per comet for a total of 640 orbits. In Section 2 we describe and present tests of our new numerical techniques. Note that it is not necessary to read this section in order to understand the results of our integrations. Those readers not interested in the numerical techniques may skip to Section 3, where the results are presented. Our concluding remarks are presented in Section 4.

2. THE RMVS METHOD

2a. Description of the Method

Until recently there has not been a tool that accurately integrates the orbits of small objects on timescales approaching the age of the solar system, while also being able to follow the important, but short-lived close approaches between these objects and planets. We have developed a new integrator for this purpose. It is based on the highly efficient symplectic algorithms pioneered by Wisdom and Holman (1991, hereafter called WH91). These techniques, and variants thereof, are now commonly called Mixed Variable Symplectic (MVS) methods (Saha and Tremaine 1993).

In the MVS method, the Hamiltonian from which the equations of motion are derived is written as the sum of two parts,

$$H = H_{\text{Kepler}} + H_{\text{Interaction}},$$

where H_{Kepler} represents the Keplerian motion of a body and $H_{\text{Interaction}}$ represents the mutual perturbations of the bodies on one another. Both H_{Kepler} and $H_{\text{Interaction}}$ are integrable (i.e., the equations derived from each Hamiltonian taken alone can be solved analytically). WH91 give explicit representations for the two Hamiltonians and show that the solution of the equations of motion for time Δt in the true Hamiltonian can be approximated to second order (Δt^2) by first applying one Hamiltonian for $\Delta t/2$, then the other for Δt, and then the first again for $\Delta t/2$. It is straightforward to show that it is not important in what order the Hamiltonians are applied.

In the N-body problem discussed here, the application of the Keplerian part of the Hamiltonian is equivalent to moving the object along a conic section. The application of the remaining part is straightforward, because the perturbation Hamiltonian is independent of the momentum and thus the positions of the particles remain unchanged while the velocities receive small kicks. The procedure works extremely well as long as the perturbations due to $H_{\text{Interaction}}$ are small. It can be generalized to higher order (Forest and Ruth 1990; Yoshida 1990; Saha and Tremaine 1993), but the higher order schemes are computationally more expensive and are superior only when very high accuracy is required (i.e., when using a much smaller timestep than is required for the statistical studies of chaotic systems described here).

The assumption that the planetary perturbations are small breaks down during a close encounter. This condition is conventionally said to occur if a body comes within one Hill radius r_{H} of the planet (cf. Lissauer 1993), where

$$r_{\text{H}} = a_{\text{p}} \left(\frac{1}{3} \frac{M_{\text{p}}}{M_{\odot} + M_{\text{p}}} \right)^{1/3}, \tag{1}$$

where a_{p} is the semimajor axis of the planet, and $M_{\odot}$ and M_{p} are the masses of the Sun and planet, respectively. Under these circumstances, the acceleration due to the planet is typically much larger than that due to the Sun. We therefore perform the MVS separation of the Hamiltonian so that the Keplerian part is centered about the *planet* rather than the Sun. In this way, we can integrate *arbitrarily* close encounters. In contrast to other methods, this algorithm is most computationally efficient during very close encounters, since the perturbations from other bodies are then sufficiently small that the orbit is very close to a conic section. Thus, a timestep can be used which is a substantial fraction of the encounter timescale.

However, a problem arises in the intermediate region between one and about three Hill radii from the planet, where the forces from the Sun and the planet are comparable. For particles in this region we perform a heliocentric MVS step, but decrease the timestep of the integration by some constant. Thus, the code employs multiple timesteps in a manner which concentrates the computational effort where it is needed.

Our experience has led us to the following two-tier approach: If a particle lies within the intermediate zone at the beginning of a normal timestep or is predicted to lie within this zone at the end of the timestep, then its timestep is decreased by a factor of n_1. If a particle lies within the Hill sphere of a planet at the beginning of a timestep or is predicted to lie within it at the end of the timestep then its timestep is decreased by *another* factor of n_2. The numerical values adopted for the timestep reduction factors are guided by experience. We have adopted $n_1 = 10$ and $n_2 = 3$. The outer radius of the intermediate zone was set at $3.5r_H$.

Our use of planet-centered coordinates during close encounters is reminiscent of, but mathematically distinct from, previous close encounter algorithms known as regularization methods (see, e.g., Stiefel and Schiefele 1971). We, therefore, call this technique the *Regularized Mixed Variable Symplectic (RMVS) Method*.

An additional point must be made. In practice, we found that when our RMVS code was run, most of the CPU time was spent in evolving the bodies under the Keplerian Hamiltonian. This procedure requires solving a differenced version of Kepler's equation (see WH91), which for planet-centered orbits typically involves unbound particles. We have adopted the algorithms involving universal variables described in Danby (1988). Several refinements were incorporated (including an improved algorithm for near-parabolic cases and a very efficient treatment of low eccentricity cases) and are available from the authors upon request.

2b. Tests of the RMVS Code

Testing of a code such as our RMVS integrator is a very complicated task since it is intended to model chaotic systems, which do not have analytic solutions. Therefore, there are no sample problems that we can run that test *all aspects* of the code against exact known solutions. Thus we pursued three avenues of approach to testing our code: (i) The individual subroutines of the code were systematically tested before incorporation into the final code. For very complex routines (such as the force calculation), independent routines were written by the two authors and the results checked to ensure that they agreed to within the computer roundoff. (ii) The few special cases for which there are conserved quantites were used as

tests. Unfortunately, such test are somewhat limited. They either involve only global parameters (such as conservation of energy), which only tests the integration of the massive bodies, or require very simple planetary systems (such as the circular restricted three body problem). We ensure that the code conserves these quantities to very high numerical accuracy in all problems of this type known to us. (iii) A suite of short time duration problems designed to test the entire RMVS code was run using our code as well as several other well-established codes. We verified that the results from our code statistically agreed with the results from the established codes in each of these cases.

There are three major sections of the code that had to be tested: the section that integrates the massive mutually interacting particles; the part that integrates the orbits of test particles that are not suffering close approaches; and the section that integrates the close approach between a test particle and a planet. We developed several tests for each of these. Overall, we spent several months designing and implementing tests that exercised all the aspects of the code. As an illustration, we now present the results of a few of these tests.

The part of the code that integrates the mutually interacting particles was tested using the initial masses and coordinates of the four giant planets and the Sun given in the classic integration of Cohen et al. (1973, hereafter called CHO73). With a timestep of 0.1 years (which is typical of that used in the simulations described below), the total energy was conserved to within one part in 10^7 and the variations in the planetary orbital elements were indistinguishable from those published in CHO73 over the common integration span of 1 Myr. However, as is typical of MVS integrators using fairly large timesteps, the exact phases of Jupiter and Saturn in their orbits were not reproduced at the end of the integration (although those of Neptune agreed to within one part in 10^4). This is unlikely to be important in our statistical study of chaotic test particles.

A further test of the mutually interacting parts of our code is presented in Fig. 1, where we compare the variation of the orbital elements of the planets in our comet integration (points) to that from a more accurate (but much more CPU-intensive) integration of the same seven-planet system using a Bulirsch–Stoer scheme (Stoer and Bulirsch 1980). The two are indistinguishable. The difference between the Earth's eccentricity in the two integrations is 10^{-5} at -10^6 years.

One of the procedures used to test the section of the code that integrates the orbits of massless test particles under the influence of, but not suffering close encounters with, the planets is to study the behavior of test particles near resonances. We take an example from Murray and Fox (1984), who integrated the orbits of test particles near
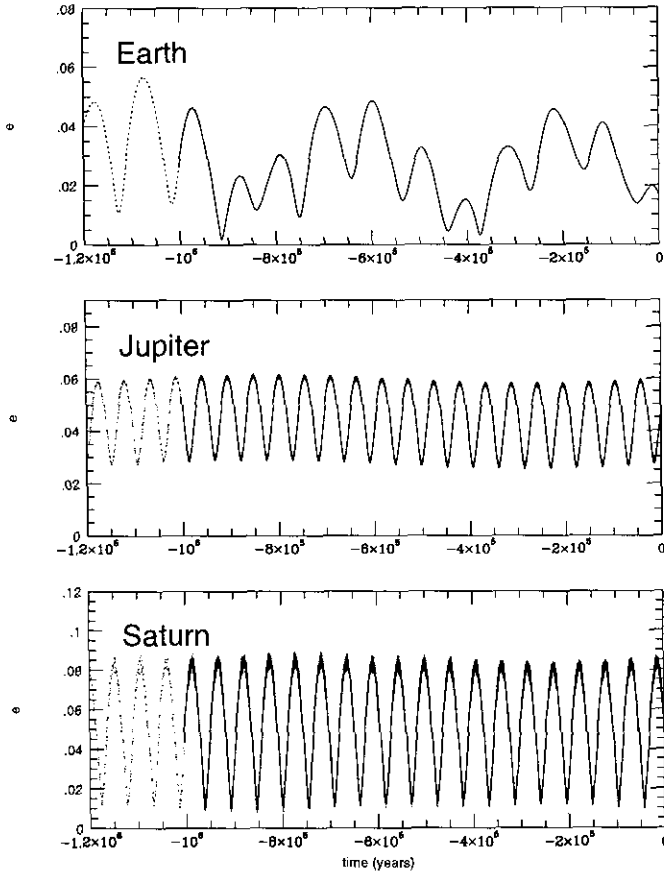
FIG. 1. The eccentricities of the Earth, Jupiter, and Saturn backward in time. The solid curves represent the results of an integration using a Bulirsch–Stoer scheme. The dotted curves represent the results using our MVS integrator.

the 3 : 1 resonance with Jupiter. In their integration, the only planet they included was Jupiter, which was on an eccentric orbit and thus had no integrals of the motion. Murray and Fox found that both regular and chaotic orbits existed near the 3 : 1 resonance. We integrated the orbits of two of their test particles, the ones shown in their Fig. 5a (regular, hereafter MF5) and Fig. 6a (chaotic, hereafter MF6). The results of our integrations of the orbits of these particles are shown in Fig. 2. Figure 2a shows the variation in the eccentricity as a function of time of MF5. The dotted and solid curves represent integrations done with our RMVS code (using a timestep of 1/40 of the test particle's orbital period) and a Bulirsch–Stoer code (using a tolerance of 10^{-8}) respectively. Note that the two are indistinguishable. They also agree very well with Murray and Fox's integrations. Figure 2b is the same as Fig. 2a but for MF6. Here the two integrations significantly diverge after about 2000 Jupiter periods. This is to be expected for chaotic orbits, especially since the Lyapunov timescale for this orbit is only ~200 Jupiter periods.

We present two illustrative examples of the accuracy

of the full RMVS code. We first integrated the trajectory of a test particle in the restricted circular three-body problem for which there exists an analytic integral of the motion, the Jacobi constant, which can be used as a check on the integration. The massive bodies had the mass of the Sun and Jupiter and remained in a circular orbit about each other with a semimajor axis of 5.2 AU. Several tens of particles were studied using a timestep of 0.01 Jupiter periods (similar to the one we employ in the simulations described below). Figures 3a and 3b show the variation of the semimajor axis (a) and eccentricity (e) for the test particle that had the largest number of close encounters with Jupiter. As shown in Fig. 3c, the observed changes in orbital elements seen in this particle were due to close approaches to Jupiter. Figure 3d shows the fractional change in the Jacobi constant during this same period of time. These tests and others suggest that the error in the Jacobi integral propagates in a manner consistent with a random walk (i.e., there is no evidence for a systematic
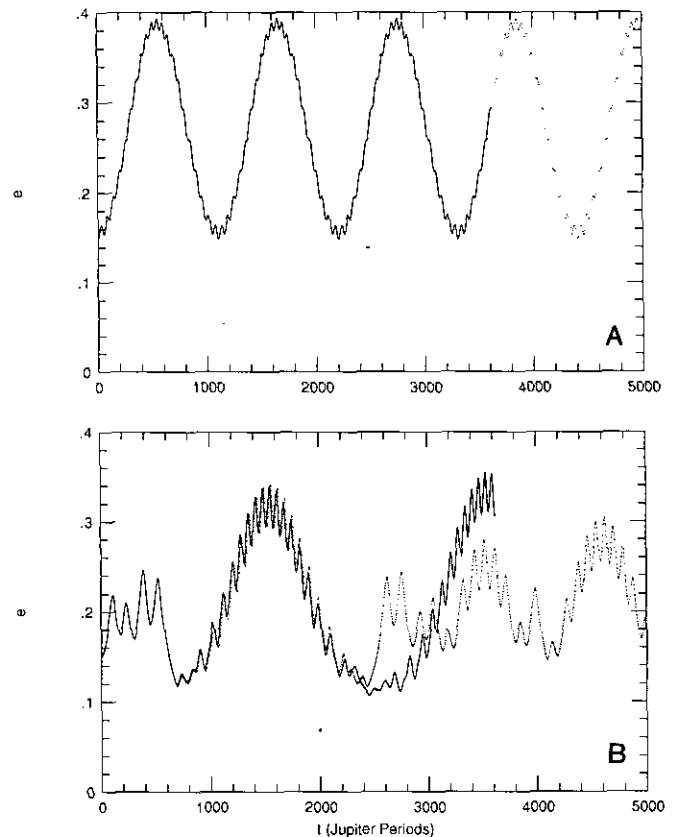

FIG. 2. The variation of eccentricity with respect to time of two particles in the 3 : 1 resonance with Jupiter. The dotted and solid curves represent integrations done with our RMVS code and a Bulirsch–Stoer code respectively. (a) An object in a regular orbit. (b) An object in a chaotic orbit. The observed divergence is expected for chaotic orbits, especially since the Lyapunov timescale for this orbit is approximately 200 Jupiter periods.
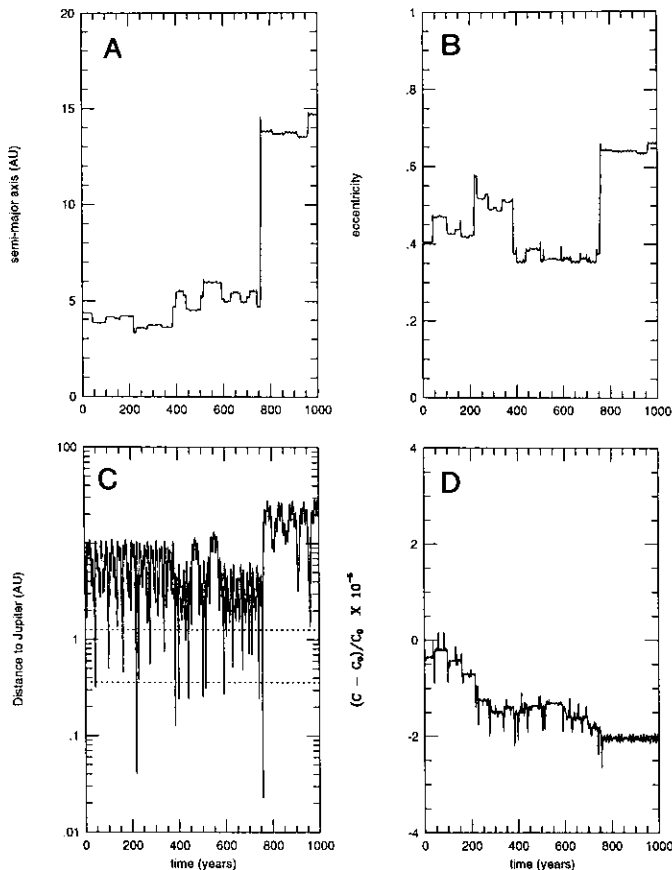
FIG. 3. Results of an integration using our new RMVS code. The behavior of a test particle on a Jupiter-crossing orbit in the circular restricted three body problem is shown. (a) The semimajor axis. (b) The eccentricity. (c) Its distance from Jupiter. The variations in the orbital elements are due to encounters with Jupiter. If the particle falls between the two dotted lines then the timestep is decreased. If it falls below the bottom dotted line, the integration is performed in a planetocentric frame. (d) The fractional error in the Jacobi constant, C.

as they leave the figure is only 2×10^{-4} AU. Figure 4c shows the same orbit calculated with the RMVS code, but with a timestep of half a year (about five times longer)! Again, this orbit is almost exactly the same as the one produced by the Bulirsch–Stoer integrator (cf. Fig. 4a).

We emphasize that the above tests are presented only as examples. Many more tests were run. In particular, a variety of further comparisons of our code with a Bulirsch–Stoer integrator were made to ensure that our rather complicated bookkeeping when dealing with swarms of test particles did not introduce any errors. In view of the chaotic nature of particles undergoing close encounters, it is obviously impossible to reproduce the details of individual orbital evolution beyond an encounter or two, but tests indicated that up to that time, each particle was accurately integrated. Furthermore, integrations of swarms for moderately long times gave similar statistical behavior in the two codes. Several other confirmations will be found in Section 3. These include showing that comet P/Machholz becomes a sun-grazer as predicted by Bailey et al. (1992) and that comet P/Encke behaves qualitatively the same in a comparison of the RMVS and the Bulirsch–Stoer integrators. It should be noted, though, that the RMVS code is typically 5–10 times faster than the Bulirsch–Stoer integrator for comparable accuracy. It is more than an order of magnitude faster than the commonly used high-order Gauss–Radau scheme (RA15, Everhart 1985).

growth in the error). Our study of many particles suggests that, with this timestep, the fractional error in the Jacobi constant is $\sim 10^{-5}$ after 10 close approaches. Thus we anticipate fractional errors of only $\sim 10^{-4}$ after 1000 close approaches.

The second test illustrates the power of the new technique. Tancredi et al. (1990) found that the comet P/ Helin–Roman–Crockett will suffer a close approach to Jupiter in the year 2075 that will lead to a temporary capture of the comet. Figure 4a shows the trajectory of the comet using a Bulirsch–Stoer integrator. The trajectory is plotted in a frame that is centered on Jupiter and rotates so that the Sun is always on the negative x-axis. Figure 4b is the same trajectory using our RMVS integrator with a timestep of 38 days—the timestep used for most of our integrations. Note that Fig. 4a and 4b are indistinguishable. Indeed, the distance between the two trajectories
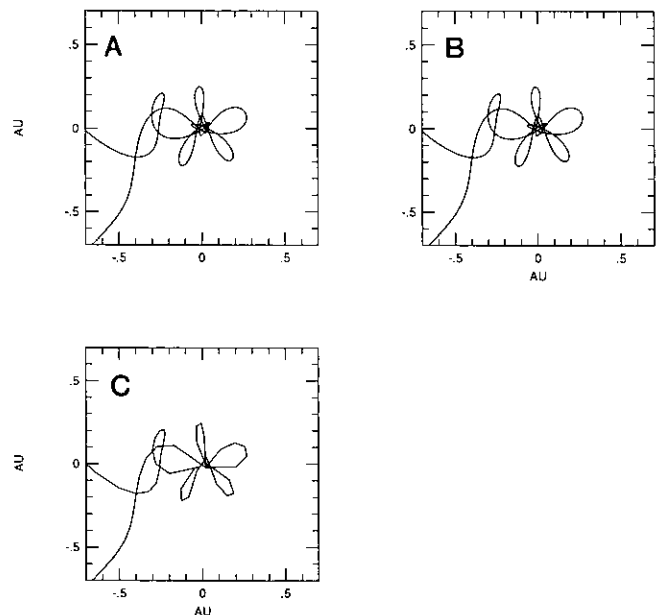

FIG. 4. The trajectory of comet P/Helin–Roman–Crockett during its 2075 A.D. encounter with Jupiter. The trajectory is plotted in a frame that is centered on Jupiter and rotates so that the Sun is always on the negative x-axis. (a) The trajectory was calculated using a Bulirsch–Stoer integrator. (b) The RMVS integrator was used with $\Delta T = 38$ days. (c) The RMVS integrator was used with $\Delta T = \frac{1}{2}$ year.

3. RESULTS

In this section, we present the results of our integration of the orbits of all known comets that are *currently* short-period. The current orbital elements for the comets and planets were kindly supplied to us by L. Wasserman and E. Bowell based on an extended version of the Marsden (1989) Catalog. In order to obtain better statistics concerning the behavior of the SPC population, four orbits were integrated for each real comet. One orbit had the initial position and velocity of the real comet, calculated from its orbital elements. The other three have initial offsets in position along the x, y, and z directions of $+0.01$ AU, respectively. This offset was chosen to account for typical uncertainties in the current orbital elements of the comets. Since their orbits are chaotic, the four orbits separate quickly and soon become independent of one another. In all, the orbits of 640 objects were calculated.

The cometary orbits are integrated under the gravitational influence of the Sun and all the planets except Mercury and Pluto. The orbits of the Sun and planets are integrated in three dimensions as a full N-body system. The comets themselves are not gravitationally interacting with each other. We did not include any nongravitational forces because it is not clear how they vary over such long time periods. We integrated the system, including the Sun, planets, and comets, forward and backward in time for 10^7 years. We continued to follow a comet until it either became unbound from the Sun and reached a distance of 150AU or became a sun-grazer. We define a sun-grazer as an object with $q < 0.01$ AU $\approx 2R_\odot$.

Before presenting the results of our integrations we must first caution the reader on two points. First, since the comet orbits are planet-crossing and thus chaotic, it is not possible to accurately determine the long-term fate of any individual object. However, it is appropriate to extract statistical information from these integrations about the behavior of this sample of comets that will resemble the evolution of the real system. For the remainder of this paper we concentrate on the statistical attributes of our integration.

Secondly, we cannot even study the long-term statistical behavior of the system of comets into the past for timescales longer than the Lyapunov time because the orbits are chaotic and because the phase space available to the objects is probably much larger than the region from which they came. To illustrate this point, consider the analogy of an initially evacuated room with rough walls and a large open window into which molecules are injected through a narrow hose. Once the system has reached a steady-state (i.e., the number of molecules entering through the hose is equal to the number leaving through the window), suppose that the position and velocity of all the particles in the room were recorded. If an attempt were made to integrate the system backwards, more particles would leave through the window than through the hose because, after several reflections off the walls, the particles would have "forgotten" their initial states. In our case, injection through the hose corresponds to injection into a visible SPC orbit, and leaving through the window corresponds to the many more avenues of escape available to a SPC. In this light, the backward integration is statistically equivalent to the forward integration and should be viewed as another example of the future behavior of the system. As a result, when we quote median timescales and percentages in what follows, we generally will quote the average of the values in the forward and backward integrations with an uncertainty which is half the difference between them (i.e., values will be presented as mean $\pm$ difference/2). As we will see, the differences between the forward and backward integrations are very small. These similarities reinforce our analogy.

Using our integration, it is possible for the first time to calculate, by direct numerical integrations, the dynamical lifetime of SPCs. The upper curve (marked "ALL") in Fig. 5 shows the number of comets remaining in the solar system as a function of time. We plot these data for both the forward (right) and backward (left) integrations. The time it takes to lose half the comets is $4.5 \pm 0.1 \times 10^5$ years. At the end of each of the 10^7 year integrations, 10 ± 4 of the original 640 objects remain. Of these remaining objects, none are on Jupiter-crossing orbits. Six of them have $a > 100$ AU and 12 have $a > 30$ AU. Most are in very eccentric orbits, but 4 have $e < 0.3$. Of these four, three are not on planet-crossing orbits; two are between Saturn and Neptune and one is between Mars and Jupiter. One object of particular note is temporarily trapped near the $1:1$ resonance ("Trojan point") with Neptune, but it leaves the resonance near the end of the integration.

Öpik (1963) calculated the expected dynamical lifetimes of 16 SPCs using a statistical semianalytic theory. His sample included a wide range of objects with periods ranging from 3.3 years (P/Encke) to 120 years (P/Swift-Tuttle). He found that the median lifetime for his sample is approximately 2.5×10^6 years. We find that this sample has a median lifetime of 4.6×10^5 years in our integrations. There is no correlation between his lifetimes and ours for individual objects. The ratio of his dynamical lifetimes to ours range in values between 0.03 and 8000. Typically, his lifetimes are an order of magnitude larger than ours.

3a. Semimajor Axis Distribution Evolution

We now discuss the evolution of our comets' semimajor axis distribution. It has been typical in the literature to divide SPCs into two families: Jupiter-family and Halley-
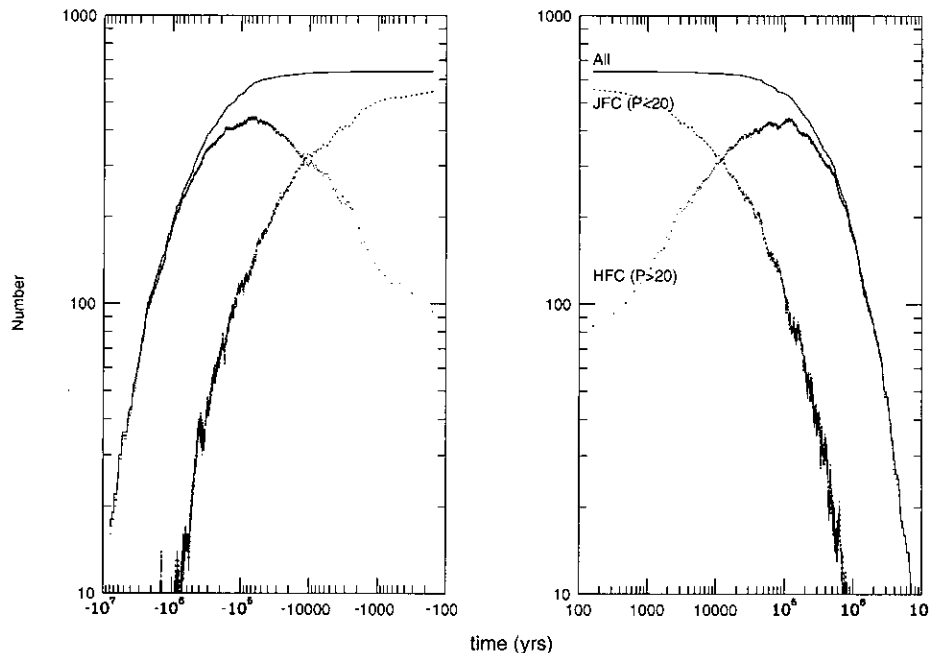
FIG. 5. The number of comets remaining in our integrations as a function of time. The solid curves represents the total number of comets. The dashed and dotted curves represent the number of Jupiter-family comets ($P \leq 20$ years) and Halley-family comet ($P \geq 20$ years) respectively. Note that we employ the JFC/HFC definition based on period in this figure.

family comets. Many authors (see, e.g., Fernández *et al.* 1992) define a classical Jupiter-family comet (hereafter JFC[P]) as one with a period less than 20 years and a Halley-family comet (HFC[P]) as one with a period between 20 and 200 years. (We use the notation "[P]" to indicate that the distinction is based on period. We show in the next section that a dynamically more descriptive classification into Jupiter and Halley families can be made using the initial Tisserand parameter rather than period). The two families defined on the basis of period can be distinctly seen in Fig. 6, which shows the current inclinations of the comets in our sample as a function of their current semi-major axes. The dotted line represents the division between JFC[P]s and HFC[P]s. It can be clearly seen in the figure that the JFC[P]s have a much flatter inclination distribution than the HFC[P]s. The mean cos (i) of the JFC[P]s is 0.951 (corresponding to $i = 18°$) while the mean cos(i) = 0.427 ($i = 65°$) for HFC[P]s.

Since the JFC[P]s tend to have more frequent and lower velocity encounters with Jupiter than the HFC[P]s, one would expect that JFC[P]s would have much shorter dynamical lifetimes. The dashed curves (marked JFC($P <$ 20)) in Fig. 5 show the number of JFC[P]s as a function of time in our integrations. The time it takes for the number of comets to decrease to half the original number is 1.69 ± 0.01 × 10⁴ years—over an order of magnitude shorter than that of the population of comets as a whole. Approximately 95% of the JFC[P]s become HFC[P]s once

they leave the Jupiter-family, while 3% are directly ejected from the solar system and 2% become Sun-grazers ($q < 0.01$ AU).

The dotted curve in Fig. 5 shows the number of HFC[P]s as a function of time. As can be seen, the number of HFC[P]s increases for the first $\approx 10^5$ years. These are objects that evolve from the Jupiter-family to the Halley-family via close encounters with Jupiter. Since the Tisserand parameter (which is a relationship between a, e, and i) is conserved for most of these objects during this encounter, afterward they must have large perihelion distances and thus they are unlikely to be observed. The mean q of objects becoming HFC[P]s from the Jupiter-family is 4.6 AU; only 5% of them have $q \leq 2.5$ AU. Note that since most of these objects are not "visible," they will not affect the observed inclination distribution of the Halley-family. Also, although the observed number of JFC[P]s is much larger than the observed number of HFC[P]s, it is clear from this discussion alone that the true number of HFC[P]s must be much larger than the number of JFC[P]s.

Our integration shows that JFC[P]s and HFC[P]s defined on the basis of period are not dynamically distinct objects. Based on period alone, the median SPC moves between the two families 12 ± 1 times. For example, Fig. 7 shows the dynamical evolution of the comet P/Temple-Swift. We must emphasize that this figure is only illustrative; it cannot be used to predict the long-term behavior
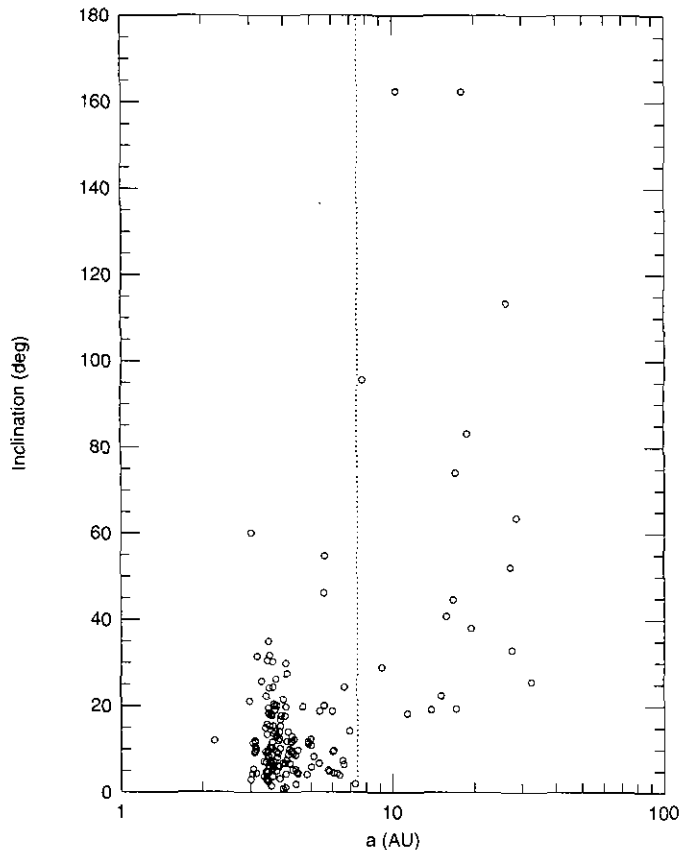
FIG. 6. The relationship between the current inclination, i, and current semimajor axes, a, for all short-period comets in our sample. The dotted line is at $P = 20$ years ($a = 7.4$ AU).

of this particular comet because its orbit is chaotic. Figure 7a shows the evolution of the comet's semimajor axis over its entire lifetime. The dashed line represents the boundary between JFC[P]s and HFC[P]s. Note that the comet moves back and forth across this boundary several times, especially in the backward integration. It is important to note that when this comet is visible, it is always a JFC[P].

In our initial sample of comets, 89% are JFC[P]s. We find that in both our integrations, 91% of all our comets become JFC[P]s at some point in their lives. Thus we predict that approximately six of the known HFC[P] comets will at some point in the future become JFC[P]s. The typical comet in our integration spends 22% of its time as a JFC[P](median value).

We have seen that a classification of SPCs into families based solely on the basis of period is not very illuminating from a dynamical point of view. We turn to a better diagnostic next.

3b. Evolution of the Tisserand Parameter

As we discussed in Section 2b, in the circular restricted three-body problem, there exists an integral of the motion

for any test particle—the Jacobi integral. Although Jupiter is not on a strictly circular orbit (nor is it the only planet), one can calculate for each comet an approximation to the Jacobi integral called the Tisserand parameter which is often found to be roughly constant during short-term integrations. Following the usual convention we define an object's Tisserand parameter to be $T = a_J/a + 2\sqrt{(1 - e^2)a/a_J} \cos(i)$, where a_J is Jupiter's semimajor axis. Note that objects with $T > 3$ cannot cross Jupiter's orbit in the circular restricted case, being confined to orbits either totally interior or totally exterior to Jupiter.

Figure 8 shows the initial value of T for each comet in our survey versus its initial semimajor axis. The vertical dotted line represents the dividing line between conventionally defined JFC[P]s and HFC[P]s. The upper curved line shows the value of T versus a for a comet with $q = 2.5$ AU and $i = 0$, while the lower curved line is the minimim possible value of T versus a for prograde orbits (corresponding to an orbit with $e = 1$ or $i = 90°$). Low-inclination objects with $q > 2.5$ AU would lie in the upper right corner of the diagram, and the apparent absence of such objects in the data is largely a selection effect since objects with perihelia beyond 2.5 AU are difficult to detect. In addition, it is not physically possible for prograde comets to lie below the bottom curve. These constraints explain what otherwise appears to be a fairly strong correlation between T and a seen in the figure and thus the correlation is not significant.

As described above, we have found that the classical distinction between Jupiter and Halley families is unenlightening, since objects switch classes frequently during their dynamical lifetimes. Carusi and Valsecchi (1987) have proposed that a dynamically more meaningful classification would be to classify a comet as being of the Jupiter family if it has $T > 2$ and of the Halley family if $T < 2$. The horizontal dashed line in Fig. 8 shows the new dividing line and we see that only three objects are reclassified under this new system (i.e., comets P/IRAS, P/Machholz, and P/Tuttle are now considered Halley-family objects.) The power of this classification lies in the fact that we find in our integrations that for most comets T is well enough conserved during their dynamical lifetimes that the vast majority of them do not change families.

Figure 9 shows a histogram of the range of variation of T during the dynamical lifetime of each comet in our forward integrations. The median change is T is 0.44 ± 0.02. We find in fact that only 8% change families during their dynamical lifetimes. Most that change are initially near the dividing line at $T = 2$—less than 2% switch from $T < 1.5$ to $T > 2.5$. As an example, Fig. 10 shows the temporal variation of T for the comet P/Tempel-Swift, whose orbital element evolution is plotted in Fig. 7. The relatively small variations in T should not be construed as implying that this comet is always totally controlled by
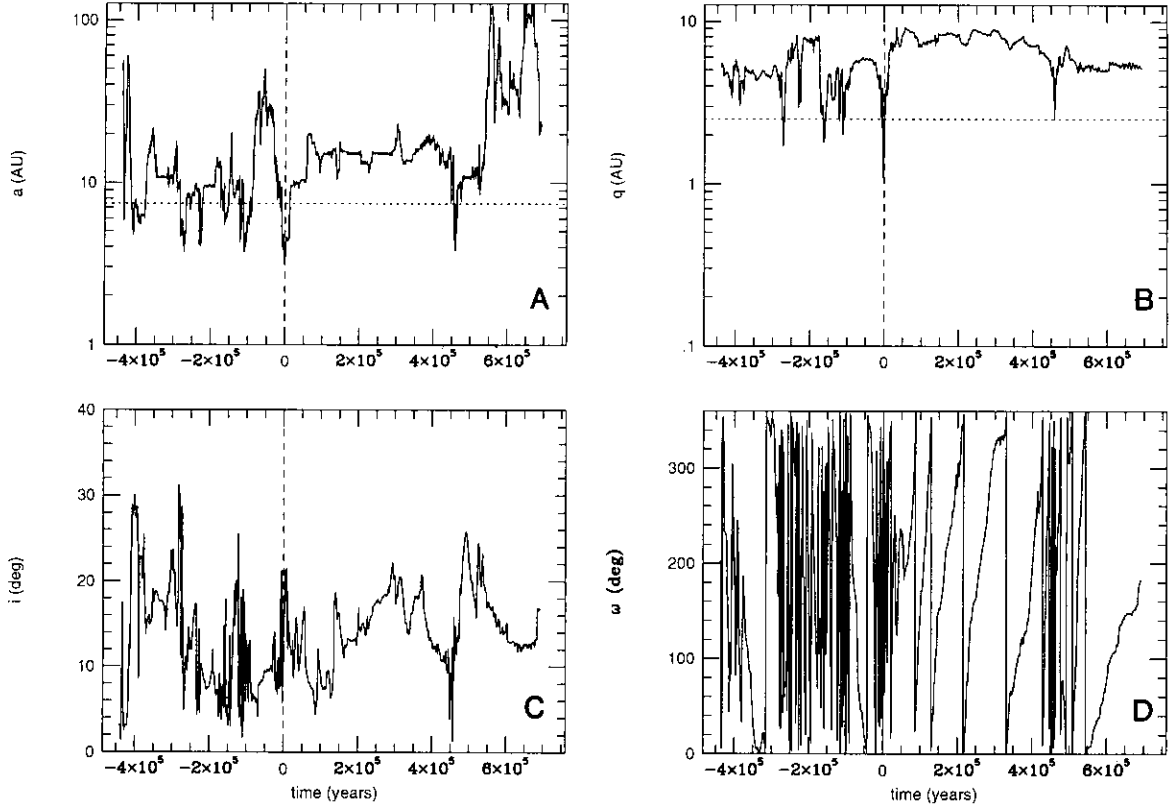
FIG. 7. The behavior of comet P/Tempel–Swift over its entire dynamical history. (a) Semimajor axis. The dotted line is at $P = 20$ years. (b) Perihelion distance. The dotted line represents the limit of visibility limit ($q = 2.5$ AU) set by Quinn *et al.* (1990). (c) Inclination. (d) Argument of perihelion.

Jupiter, however. Indeed, the comet spends considerable time with pericenter nearer to Saturn's orbit than Jupiter's in an orbit which is dynamically similar to Chiron's (for which $T = 3.35$). Objects with $q > 6$ AU cannot come within Jupiter's Hill sphere and so cannot suffer a strong encounter with the planet. For the entire set of comets, the median fraction of time spent as a JFC with $q > 6$ AU is 48%, so Chiron-like phases are quite common. This illustrates one drawback of the new classification—some comets in the solar system that are not crossing Jupiter will be classified as JFCs. Clearly, some modification of this definition is in order. Perhaps including only objects with $T \lesssim 3$ or adding a condition based on the appearance of their orbits (such as their being Jupiter-crossing) is appropriate. We will leave this topic to future discussions and will continue employing the definition stated above.

As we have mentioned, only a modest fraction of comets change families in the new classification scheme, so it is appropriate to reexamine the issue of the dynamical lifetime against ejection or sun-grazing of the comets in the simulation. This is shown in Fig. 11, where we see that the median lifetime of the JFCs is $3.25 \pm 0.06 \times 10^5$ yr. By contrast, the median lifetime of the HFCs is about three times longer, $1.00 \pm 0.01 \times 10^6$ years.

In general, we find the advantages of a classification based on the initial Tisserand criterion to be very compelling. So, although there are some problems with the definition suggested by Carusi and Volsecchi (1987), we adopt it in what follows.

3c. Perihelion Distance Evolution

The current perihelion distance distribution of comets is strongly peaked toward small values. This is most likely due to a strong observational bias against the discovery of comets with large perihelion distances because they are less active and do not pass close to the Earth. Quinn *et al.* (1990) define a "visible" comet as one with $q \leq 2.5$ AU. If a comet has a q greater than this value then, they argue, it is not likely to become bright enough to be discovered. Indeed, only 14% of the known short-period comets have q larger than this value and none of them are HFCs. For this paper, we adopt this definition of visibility.

We find that the perihelion distance of a comet can change drastically over its lifetime. In both our forward and backward integrations, the typical comet is visible ($q < 2.5$ AU) for only 7% (median value) of its lifetime during which it becomes visible a total of 10 times. For
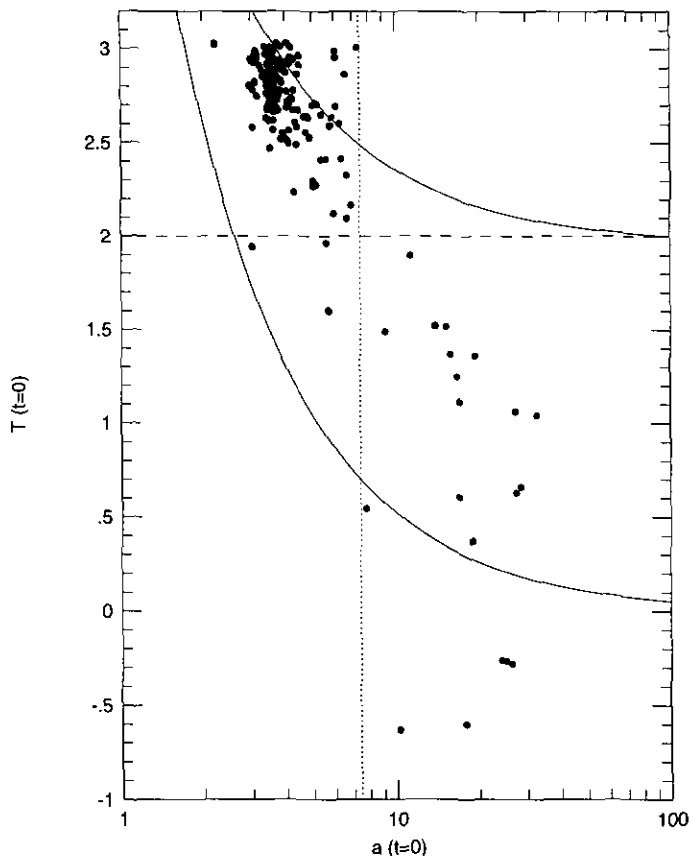
FIG. 8. The initial value of T for each comet in our survey as a function of its initial semimajor axis. The vertical dotted line is at $P = 20$ years. The horizontal line is at $T = 2$. The upper solid curve shows the value of T versus a for a comet with $q = 2.5$ AU and $i = 0$. Comets above and to the right of this line have $q > 2.5$ AU and thus are difficult to detect. The lower solid curved line is the minimum possible value of T versus a for prograde orbits. It is not possible for prograde objects to fall below this line.

example, Fig. 7b shows the evolution of the perihelion distance of the typical comet P/Tempel–Swift. The dashed line in the figure represents the visibility boundary. Notice that the comet becomes visible and invisible several times during its lifetime, using the criterion based on q.

In Fig. 12a we show a histogram of the time at which each comet that *begins* with $q < 2.5$ *first* evolves either to an orbit with $q > 2.5$ or changes family. The solid histogram is for all SPCs, the dotted histogram refers to JFCs, and the dashed histogram to HFCs. The median time for this to occur in each group is given in the first row of Table I.

In Fig. 12b we plot histograms for the same groups of the *integrated time* spent in a "visible" state (i.e., with $q < 2.5$). The second row of Table I gives the median integrated time with $q < 2.5$ for the three groups.

One of the most interesting aspects of the perihelion

distance evolution is that a surprisingly large number of comets (6% of the comets in the forward integration and 5% of the comets in the backward integration) become sun-grazers, which we define as $q < 0.01$ AU $\approx 2R_\odot$. We find that comets of either family can become sun-grazers. Indeed, sun-grazing comets can have semimajor axes between 2 and 28 AU.

Bailey *et al.* (1992) noted that there is a class of orbits which show relatively short-lived phases in temporary sun-grazing states with extremely small q. The objects in this class spend the majority of their time at inclinations near 90° and in much less eccentric orbits. Bailey *et al.* (1992) point out that comet P/Machholz is a typical example of this class and indeed we find that it and its clones exhibit this behavior in our simulations. Figure 13 shows the behavior of ω, q, and i as functions of time for P/Machholz. Note that the plunge to small q occurs as ω passes through 90° or 270°.

The sun-grazing behavior described in the work of Bailey *et al.* can be understood as a secular effect due to the influence of Jupiter alone. By averaging over the mean motions of both Jupiter (when approximated as
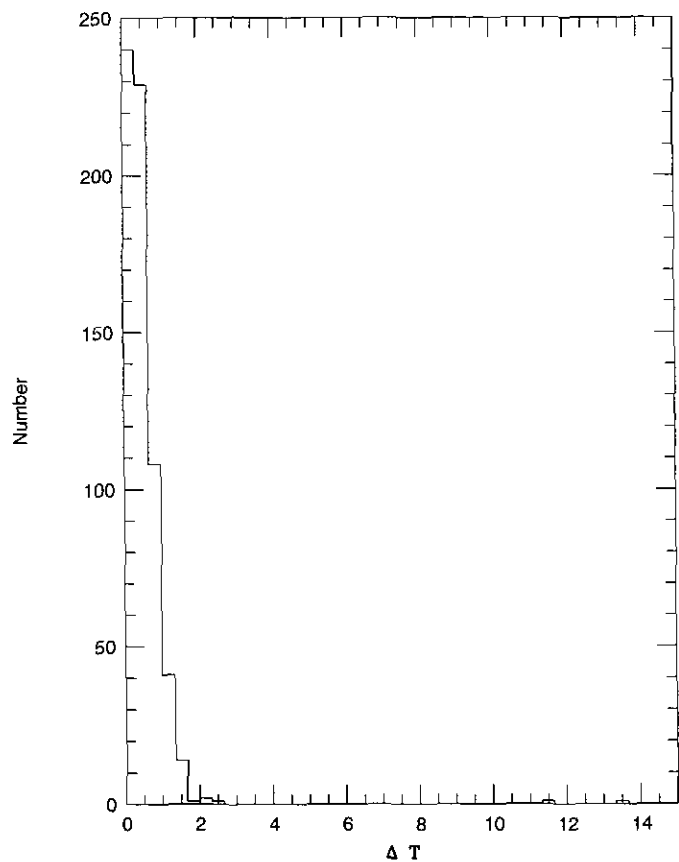

FIG. 9. A histogram of the range of variation of the Tisserand parameter during the dynamical lifetime of each comet in our forward integration. The median change in T is 0.42.
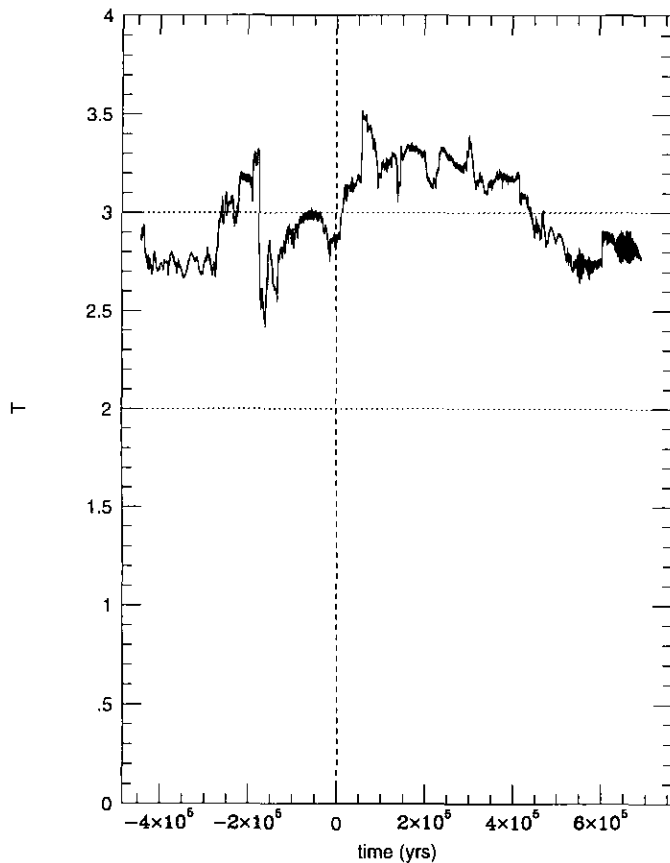
FIG. 10. The behavior of the Tisserand parameter of comet P/Tempel–Swift (see Fig. 7) over its entire dynamical history. The bottom horizontal line ($T = 2$) represents the proposed boundary between Jupiter-family comets and Halley-family comets. Orbits above the upper horizontal line do not cross the orbit of Jupiter.

roughly 6% become sun-grazers at some point in their forward evolution. (Indeed P/Halley and one of its three clones become sun-grazers in our integrations.) However, only P/Machholz begins in an initial state which allows its perihelion distance to evolve to less than 0.1 AU via the averaged effects of Jupiter alone.

Comet P/Encke is an interesting example of a comet which becomes a sun-grazer over a much longer timescale than P/Machholz and only after a long period of what appears to be a secular decrease in q. The evolution of its orbital elements is shown in Fig. 14. Note that the high frequency jitters seen in the plots of q and i are in fact the analytic secular oscillations described above. The long-term variations seen in the figure are the eventual cause of P/Encke becoming a sun-grazer. It is striking that the inclination swings from nearly zero to 180° and back several times during the integration and that the eccentricity of the comet is 1.000 when $i = 90°$. Furthermore, the three clones of P/Encke also became sun-grazers and showed qualitatively similar long-term variations in i and q

As a check on the sensitivity of P/Encke's orbit to initial conditions, we integrated 19 additional Encke clones which were initially offset in position by $\sim 10^{-7}$ AU in random directions. We found the same sort of behavior for all these objects even though the Lyapunov timescale for P/Encke was calculated to be about 100 years, while the median lifetime before becoming a sun-grazer was $\sim 1.4 \times 10^5$ years. Nor are the results an artifact of the RMVS code, since integrations of P/Encke's orbit (and its 19 clones) with a Bulirsch–Stoer code showed the same behavior with the same median lifetime. There are several other comets in our catalog which show evolution in q and i which drives the orbit into the sun-grazing phase. However, most do not show smooth, apparently secular drifts for as extended a period as P/Encke. This is because of close approaches to planets. An analytic explanation for this long-term "secular" behavior remains a problem to be pursued in the future. Valsecchi has pointed out that P/Encke may be currently near the ν_6 secular resonance. However, this is not certain because the locations of the secular resonances are not known for eccentricities as large as P/Encke's (cf. Morbidelli and Henrard 1991).

Finally, let us consider the case of Near-Earth Objects, which have been classified as objects with $q < 1$ and $T > 3$ (i.e., Earth-crossing but not Jupiter-crossing; see, e.g., Weissman et al. 1989). Note that P/Encke is currently part of that population. We find in our simulations that 3 ± 1 of the 640 SPCs that were not initially NEOs spent some fraction of their dynamical lifetimes as NEOs. For these objects, the total time spent as an NEO was 10^3–10^5 years. Thus, SPCs can be a source of at least some of the NEOs (also cf. Wetherill 1991).

if it were on a circular orbit) and the comet, the resulting equations of motion for the comet admit three integrals of the motion—the semimajor axis a, the square of the component of angular momentum perpendicular to Jupiter's orbit (conventionally written as $\Theta = (1 - e^2)\cos^2 i$), and a third integral which is essentially the averaged Hamiltonian, K(Quinn et al. 1990, Bailey et al. 1992). For the case in which the comet's semimajor axis is much smaller than Jupiter's the third integral is given by $K = e^2(5 \sin^2 i \sin^2 \omega - 2)$. Obviously, the range of variations in q is set by the values of the integrals at any given time.

In the real Solar System the values of the approximate integrals change either gradually due to the secular effects of the other planets, or occasionally rapidly due to strong encounters with a planet. P/Machholz is an extreme example in that it begins in a nearly sun-grazing orbit and its values of the approximate integrals become those of a sun-grazer within a time of only three times the period of precession of ω. Of the comets in our simulation,
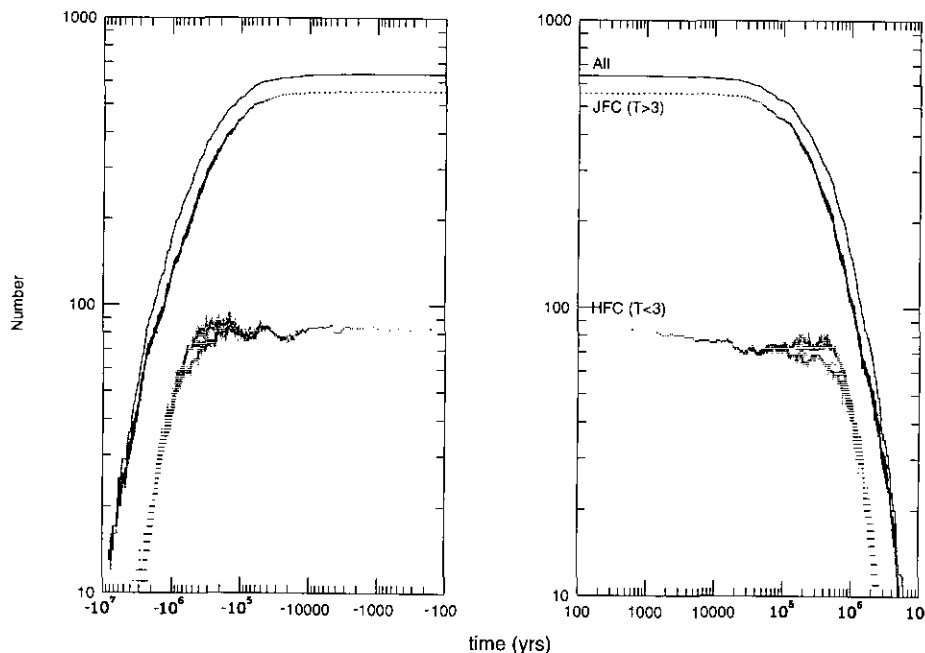
FIG. 11. The number of comets remaining in our integrations as a function of time. The solid curves represents the total number of comets. The dashed and dotted curves represent the numbers of Jupiter-family comets ($T > 2$) and Halley-family comets ($T < 2$) respectively. Note that we have employing the JFC/HFC definition based on the Tisserand parameter in this figure.

3d. The Evolution of the Inclination Distribution

In this subsection we discuss the behavior of the inclination distribution of the SPCs. As discussed earlier, Fig. 6 shows that the HFCs and the JFCs have very different inclination distributions. Of particular importance is the very flat inclination distribution of the JFCs. It has been argued that much of the inclination difference may be due to observational biases in the discovery of these objects (Kresák 1981). However, Shoemaker and Shoemaker (1993, hereafter SS93) have argued that since comets with $q \lesssim 1$ AU are not strongly affected by observational biases and since the differences in inclination distribution persist when only these objects are considered, the differences seen for the complete sample cannot be entirely due to observational biases.

The observed differences in the inclination distributions have been at the center of the controversy over the origin of SPCs and have been used to argue that JFCs and HFCs are dynamically distinct systems that have different origins (see review by Levison 1991). Quinn et al. (1990) argue that while HFCs are most likely captured long-period comets, it is not possible to reproduce the very flat distribution of JFCs in this manner. They argue that JFCs must have come from a source that is intrinsically flat. They suggest that the source is a trans-Neptunian belt of comets as first proposed by Fernández (1980)—the Kuiper belt. However, SS93 point out that some meteor streams (Olsson-Steel 1988) and some extinct comets are

observed with semimajor axes similar to JFCs but high inclinations. Thus, they argue that high inclination JFCs must exist which have remained undiscovered. SS93 further argue that the existence of these high inclination JFCs is inconsistent with the Kuiper belt being the source for most of these objects.

SS93 also present an alternative to the Kuiper belt scenario. They argue that perhaps most visible JFCs are objects which behave like P/Machholz (see our discussion of the behavior of the sun-grazing phenomenon in Section 3c). That is, although they are most easily discovered at small q when they have small i, they may actually spend most of their time at high inclination and much larger q where they are not be active. If so, the observed very flat distribution in i for the visible JFCs would be a misleading result due to a strong selection effect. Thus, understanding the dynamical evolution of these high inclination objects is pivotal to the question of whether the Kuiper belt is the source of JFCs. We will concentrate on this question in the remainder of this subsection.

Figure 15 shows the mean cosine of the inclination of the surviving JFCs as a function of time for both our forward and backward integrations. The solid curve shows this value for all comets in the family, while the dotted curve includes only the visible members ($q < 2.5$ AU). The data for the HFCs are not presented because the mean $\cos(i)$ does not significantly change over the integrations. As discussed above, the symmetry seen in
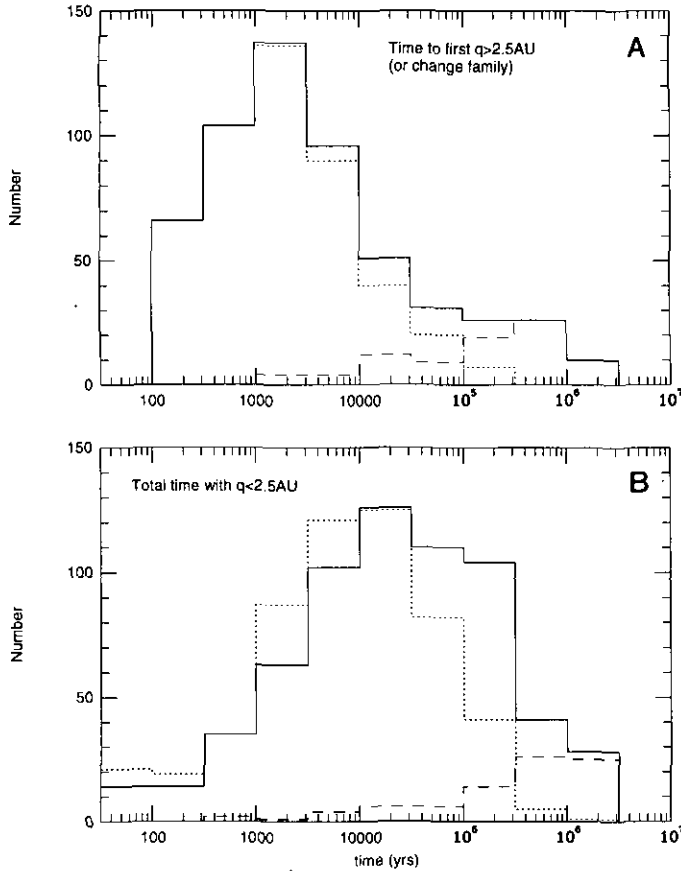
FIG. 12. Histograms of the visible lifetimes of objects in our forward integration. (a) The solid histogram shows the distribution of the time it takes for comets that begin with $q < 2.5$ to first evolve onto orbits with $q > 2.5$ (or are ejected from the solar system). The dotted curve shows the distribution of the time it takes for comets that are initially visible JFCs to evolve onto orbits that are either HFCs or have $q > 2.5$ (or are ejected from the solar system). The dashed curve shows the same for HFC. (b) The solid histogram shows the distribution of total length of time that the comet spends with $q < 2.5$. The other histograms shows the distribution of the total length of time they spend as a visible JFC (dotted) and HFC (dashed).

this diagram is due to the chaotic nature of the orbits. In an infinitely accurate calculation with infinitely precise initial conditions and non-gravitational forces, all our comets could be traced back to their origin. Since the orbits are chaotic and diverge exponentially in time, it is not possible to recover their initial distribution.

TABLE I

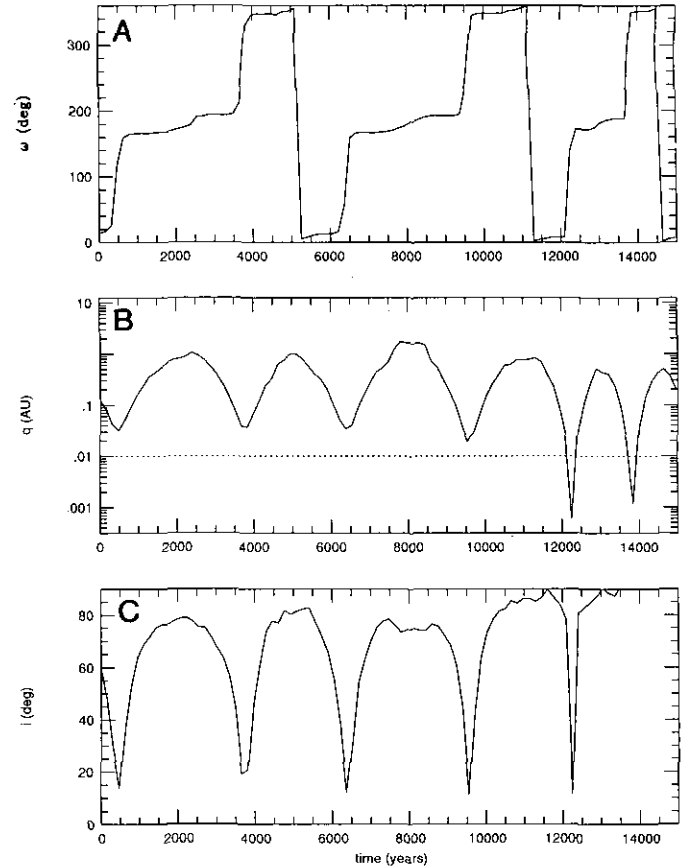|	All	JFC	HFC
Time to first $q > 2.5$ AU	1.5×10^3	1.0×10^3	1.9×10^5
Total time visible	9.6×10^3	8.5×10^3	4.4×10^5

Note. Times are in years.

FIG. 13. The temporal behavior of comet P/Machholz. (a) Argument of perihelion. (b) Perihelion distance. The dotted line is at 2 solar radii. (c) Inclination.

Perhaps the most significant result seen in Fig. 15 is that the inclination distribution of the visible Jupiter-family comets thickens as a function of time on timescales on the order of 10^4 years. These data suggest that the inclination distribution of dynamically older visible JFCs is less flat than that of younger comets. Here we define "dynamical age" as the length of time since the comet was first injected onto an orbit with $T > 2$ and $q \leq 2.5$. In addition, this result implies that if comets physically age and become extinct, the resulting distribution of extinct visible JFCs will have a more extended inclination distribution than the active ones.

It is possible to predict the number of extinct visible JFCs and their inclination distribution using our integration. The details of this calculation are given in Appendix A and the results are shown in Fig. 16. Figure 16a shows the ratio of extinct to active visible JFCs as a function of the physical fading time of a JFC. Since it is believed that the fade time is between ~2000 and ~10,000 years (cf. Rickman 1991), we predict that this ratio is between 5 and 20. The number of visible JFCs currently in our sample is
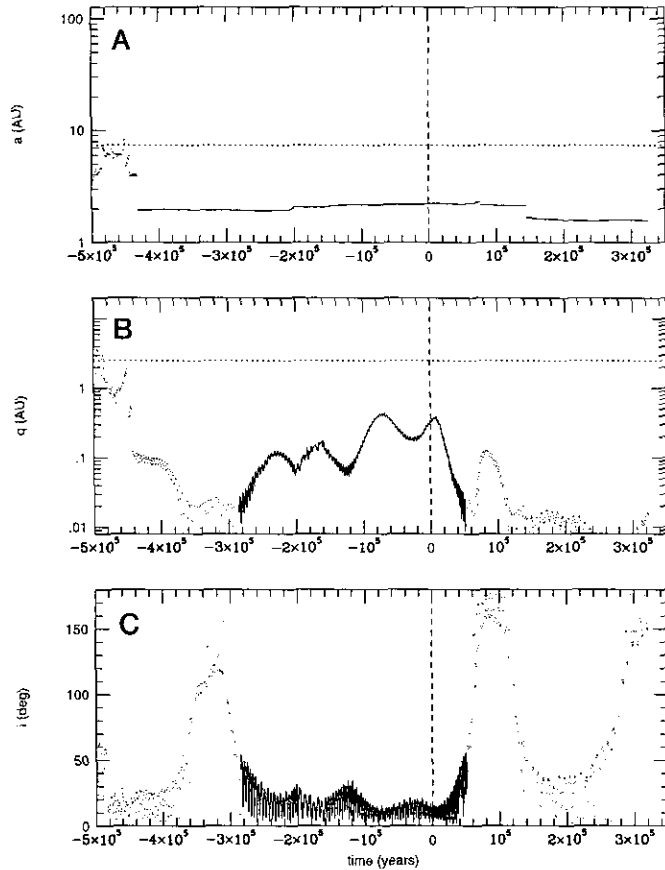
FIG. 14. The temporal behavior of comet P/Encke. The solid and dotted curves represent the periods of time "before" and "after" the comet becomes a sun-grazer, respectively. (a) Semimajor axis. The dotted line is at $P = 20$ years. (b) Perihelion distance. The dotted line represents the limit of visibility limit ($q = 2.5$ AU) set by Quinn *et al.* (1990). (c) Inclination.

FIG. 16. Predictions concerning the extinct population of JFCs. (a) The predicted ratio of extinct to active JFCs with $q \leq 2.5$ AU as a function of the fade time for comets. (b) The predicted mean $\cos(i)$ as a function of the fade time for the extinct visible JFCs (dotted curve) and the combination of active and extinct visible JFCs (solid curve). The mean $\cos(i)$ of the known active visible JFCs is included as a reference.
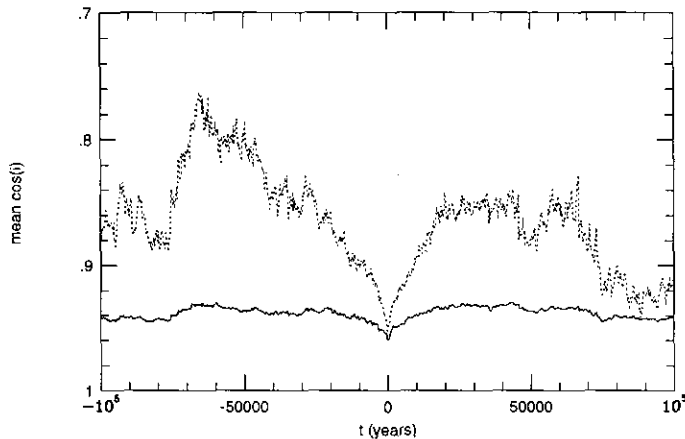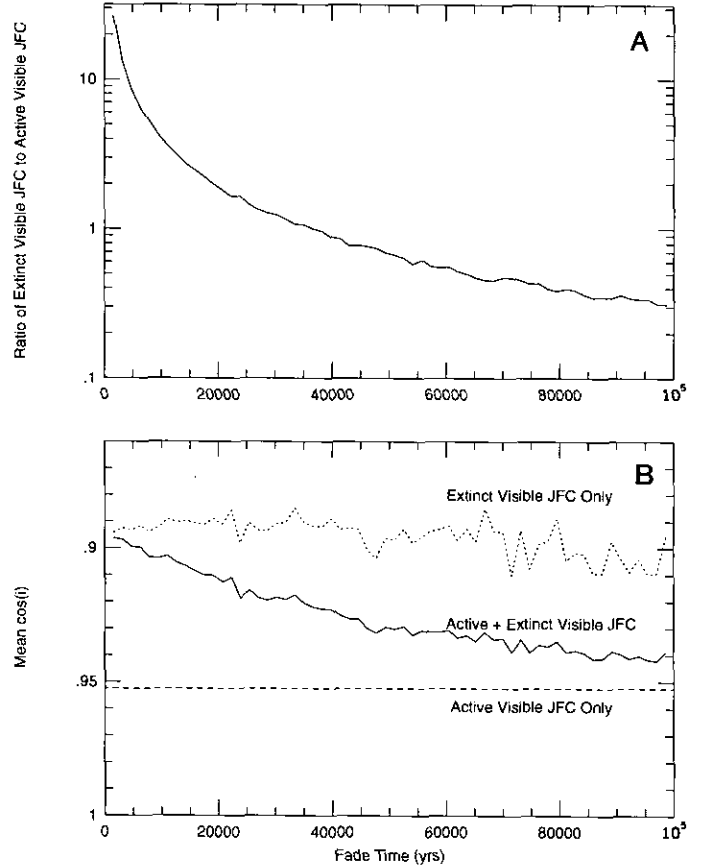

FIG. 15. The mean cosine of the inclination of remaining JFCs as a function of time for both the forward and backward integrations. The solid curve is all JFCs. The dotted curve is just those JFCs with $q \leq 2.5$ AU (i.e., "visible" JFCs).

116, so we predict that there are between 600 and 1200 extinct JFCs with $q \leq 2.5$ AU. Figure 16b shows the mean $\cos(i)$ for the comets which are active, extinct, and a combination of both for the visible JFCs as a function of fading time. Note that the predicted mean $\cos(i)$ of the extinct objects is ~ 0.89 and is approximately independent of the fade time for fade times larger than a few thousand years. This value corresponds to an inclination of $27°$. SS93 present a table of the orbital elements of all the known extinct SPC candidates. Of the 15 discovered objects, all of them have $q < 2$ AU and 14 have $2 \leq T \leq 3$ and $4° < i < 42°$. The mean $\cos(i)$ for the latter subsample is 0.881, which agrees very well with our prediction.

Although we have shown that a population of extinct high inclination JFCs does arise from a flatter distribution of active comets, we have not addressed the question of the origin of the high inclination objects. There are three possible reasons for this condition to exist: (i) a secular

$i - q$ evolution of comets exists so that they are visible only when at low inclinations (SS93), (ii) low inclination visible JFCs are removed from the visible Jupiter-family earlier than high inclination ones, and (iii) JFCs are scattered to higher inclination due to encounters with the planets. As stated above, if the first scenario is correct, then JFCs come from a distribution that is much thicker than the observed JFCs. This scenario is therefore more consistent with the Oort cloud than with the Kuiper belt as the source of the JFCs. If either the second or the third scenario is correct, then the source of the observed JFCs is as flat as or flatter than the observed JFCs. This is more consistent with the Kuiper belt than with the Oort cloud as their source. We now investigate each of these explanations separately.

(i) As discussed above, it might be argued that perhaps most visible JFCs are objects which evolve in q and i like P/Machholz. That is, they have small perihelion distances only when their inclination is small. If so, the observed very flat distribution in i for the visible JFCs would be misleading. We present two lines of arguments that show that very few SPCs are currently in states like that of P/Machholz.

First of all, our discussion of the sun-grazing phenomenon showed that the state of low i and small q occurs when the argument of perihelion ω is near 90° or 270°. (Quinn *et al.* 1990, Bailey *et al.* 1992). In reality, visible SPCs have a distribution in ω which is strongly peaked near 0 and 180° (see Section 3d), which is clearly inconsistent with most comets evolving from a much higher inclination via this mechanism.

Second, the existence of the three approximate integrals in our earlier discussion allows us to calculate the range in i and q induced by the averaged behavior of Jupiter. Figure 17 shows the results of that calculation, where a dot indicates the current values of i and q for each prograde comet and the line through each dot gives the range of those quantities predicted by the theory. Except for P/Machholz, P/IRAS, and P/Tuttle (which are represented by the three curves in the upper left of the diagram), the comets are not generally expected to vary appreciably in q due to the averaged effects of Jupiter alone. Furthermore, it appears that most of the objects have actually been found near the *peaks* of their expected ranges in i. This is to be expected from the theory, which predicts (in the absence of observational biases) that an object spends most of its time near maximum i and q and quickly passes through $i = 0$. There is no object in the known sample of SPCs for which we expect the averaged effects of Jupiter to cause a significant increase in its inclination and perihelion distance. Thus, the selection effect proposed by SS93 does not appear to explain the observed flattened distribution of visible JFCs.

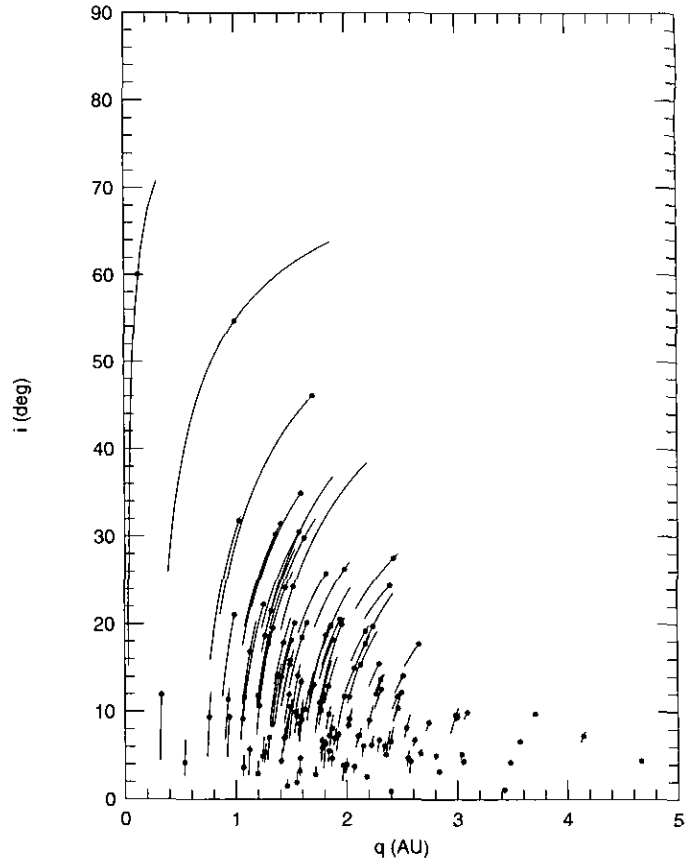It might still be argued that this simple analytic theory

FIG. 17. The evolution of perihelion distance and inclination (solid curves) for all SPCs based the secular effect due to the influence of Jupiter alone (Bailey *et al.* 1992). The dots show the current location of these comets.

does not accurately predict the behavior of the JFCs, and that there may be another secular effect that produces a strong correlation between q and i. If such an effect existed then there should be an observed correlation between a comet's inclination and its perihelion distance in our integration. In particular, objects with large q should have high i. We test this hypothesis by first dividing perihelion distance into 10 equally spaced bins for $q < 5$ AU. During the integration, we record the inclination of every comet as a function of its current perihelion bin. Figure 18a shows the mean cosine of the inclination of all JFCs within a bin as a function of the bin's mean perihelion distance. If this theory were correct, we would find that larger values of q would imply larger i. This trend is not observed. Thus, the conjecture of SS93 is not consistent with our integration.

(ii) Another possible explanation for the increase in inclination observed in our integration is that low inclination objects may have shorter dynamical lifetimes than objects with large i. If so, the low inclination objects would be removed first from the system and thus the
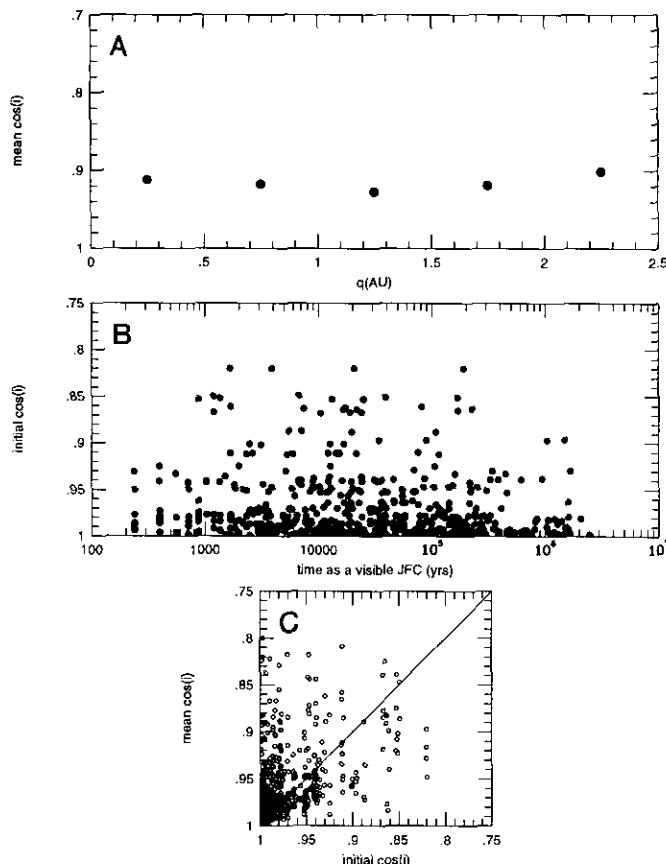
FIG. 18. (a) The mean cosine of the inclination of all visible JFCs within a perihelion bin as a function of the bin's mean q. Only comets on prograde orbits are included. (b) The mean cosine of the inclination of an individual comet as a function of the total length of time that the comet remains a visible JFC. (c) The $\cos(i)$ of an individual comet averaged over the time when it is a visible JFC as a function of its current observed $\cos(i)$.

population's mean inclination would increase. To test this possibility, in Fig. 18b we plot the initial inclination of each comet as a function of the total length of time spent as a visible JFC. If this scenario were true, we would expect to see a correlation between a comet's lifetime and its inclination, which is not observed.

(iii) The final explanation is that the orbits of individual comets may tend to evolve to higher inclinations due to nonsecular effects such as close approaches to the planets. In this scenario, the decrease in the mean $\cos(i)$ (increase in mean i) observed in the system is a result of dynamical relaxation. If this were correct, then we would expect that, on average, the mean inclination that a comet has during its time as a visible JFC would be larger than its current inclination. In Fig. 18c, we plot these two values for the 640 comets in our integration. Approximately 71% of the comets fall above the diagonal line, implying that, on average, the inclination of a comet *does* increase with respect to time.

Thus it appears that the reason that the mean inclination of our sample of comets increases is because the inclination of individual comets tend to increase. In addition, this increase is not due to known secular effects coupled with observation biases. This type of behavior can be seen in the orbit of the comet P/Tempel–Swift. Figure 7c shows the inclination of this comet as a function of time. Note that the inclination seems to vary in a manner consistent with a random walk. This supports the conclusions of Quinn *et al.* (1990) that comets injected into the visible Jupiter-family must be in low inclination orbits.

3e. Other Orbital Elements

JFCs have two interesting characteristics in their orbital element distribution that must still be discussed. These are shown as the solid histograms in Fig. 19. Figure 19a shows a histogram of the aphelion distances of JFCs, Q, which are strongly peaked near the semimajor axes of Jupiter. Approximately 73% of them have Q between 4.2 and 6.2 AU. Figure 19b shows a histogram of the argument of perihelion, ω. It can be seen that the argument of perihelion is strongly concentrated near 0 and 180°. Approximately 74% of known JFCs have ω within 45° of these two values. A value of $\omega = 0$ or 180° implies that when the comet passes through the plane of the solar system, it is also at either perihelion or aphelion.

It is easily shown (Kresák 1981) that a comet coming in from the outer regions of the solar system that is scattered by Jupiter into an orbit with $q \lesssim 2.5$ AU must have $5 \approx Q \lesssim 6$ AU, because of the approximate conservation of the Tisserand invariant during the encounter. In addition, since these comets have had a recent encounter with Jupiter, and since their Qs are approximately equal to the semimajor axis of Jupiter, then the comet must be very near the plane of the solar system when it is at aphelion. This implies that ω is approximately 0 or 180° (e.g., see Kresák 1981). This suggests that most of the JFCs have just recently been captured into the visible Jupiter-family via a close approach to Jupiter.

The above conclusion is confirmed by the behavior of the Q and ω distribution of our comets as a function of time. Figures 19a and 19b show the Q and ω distribution for visible JFCs at various times in our integration. The dotted histogram represents the distribution 2000 years in the future and the dashed histogram at 20,000 years in the future. The amplitude of the peaks in both figures substantially decreases in 20,000 years. Thus the peaks in the observed distribution imply that the observed population of JFCs is not in a steady state. This can also be seen in Fig. 7d, which shows the temporal behavior of the argument of perihelion for the comet P/Tempel–Swift. There is no tendency for the comet to have ω close to 0 or 180°. Indeed, over almost all of its lifetime ω circulates rather than librates.

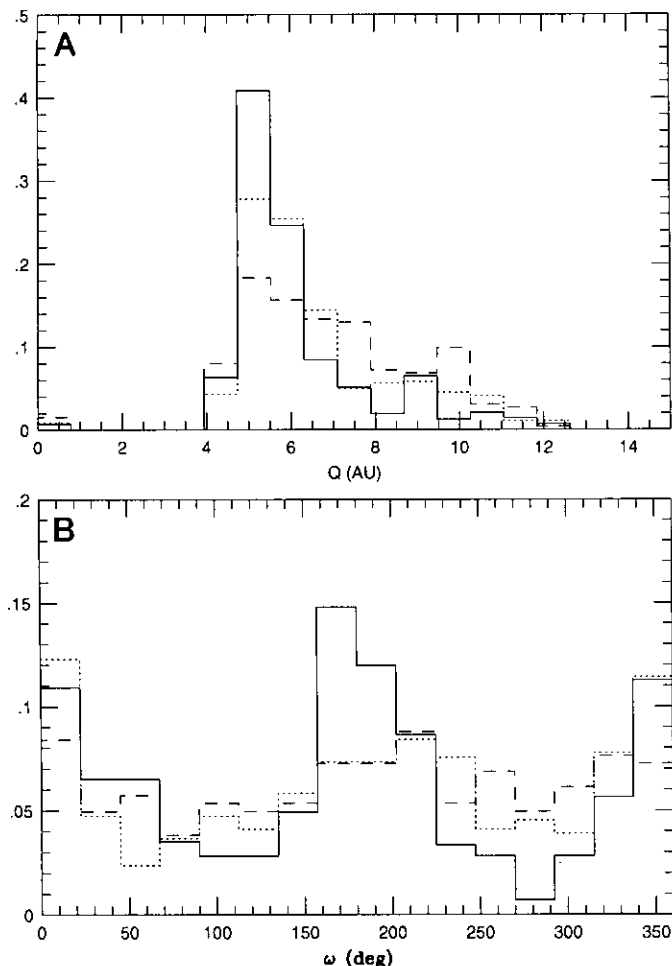The only possible explanation for the observed strong

FIG. 19. The orbital element distribution of Jupiter-family comets at three times in our integration. The solid histogram shows the current distribution. The dotted histogram represents the distribution at 2000 years in the future and the dashed histogram shows the distribution 20,000 years in the future. (a) Histogram of the aphelion distance. (b) Histogram of the argument of perihelion.

concentration of orbital elements is that many of the observed JFCs are objects that have only recently been scattered into the visible Jupiter-family. The observed peaks in Q and ω implies that most of the visible JFCs have recently suffered a close approach with Jupiter. This idea is consistent with several previous numerical integrations (Karm and Rickman 1982, Tancredi and Lindgren 1992). Note that this result does not supply any information about the number of times that comets have visited the visible Jupiter-family before the present one, and thus we cannot conclude anything about the dynamical age of the observed comets.

IV. CONCLUSIONS

We have developed and carefully tested a new integrator for solar system dynamics that is roughly an order

of magnitude faster than previously existing methods. We have used the code to integrate backward and forward the orbits of all the current short-period comets (hereafter SPCs) for up to 10^7 years under the influence of the Sun and all the planets except Mercury and Pluto. Four orbits were integrated for each comet, slightly varying the initial positions of the clones. Our key results are as follows:

(1) The median dynamical lifetime of an SPC (as measured by the length of time before half are ejected or become sun-grazers) is $4.5 \pm 0.1 \times 10^5$ years.

(2) If defined solely on the basis of period, Jupiter-family comets ($P < 20$ years) and Halley-family comets ($20 < P < 200$ years) are not dynamically distinct objects. When classified in this way, a comet moves between the families a median of 12 ± 1 times in its dynamical history. This is consistent with the results of other authors who performed integrations over much shorter periods of time (Lindgren 1991, Nakamura and Yoshikawa 1991).

(3) If defined on the basis of the Tisserand parameter T with respect to Jupiter (Carusi and Valsecchi 1987), Jupiter-family comets (JFCs, $T > 2$) and Halley-family comets (HFCs, $T < 2$) tend to be dynamically distinct. It is striking that over 92% remain in the same Tisserand family throughout their dynamical lifetimes, and that the vast majority of those that do change families tend to remain near the dividing line throughout.

(4) The median number of times that JFCs change from orbits with $q < 2.5$ to $q > 2.5$ is 10. A typical comet spends less than 7% (median value) of its dynamical lifetime with $q < 2.5$. Since objects with perihelia beyond 2.5 AU are difficult to detect, this implies that there are more than 10 times more undetected JFCs than there are visible JFCs. Of those visible now, half will evolve to states with $q > 2.5$ in roughly 10^3 years.

(5) A surprising fraction ($5.5 \pm 0.8\%$) of comets become sun-grazers. Of particular note, we predict with high probability that P/Encke will become a sun-grazer. The median lifetime of P/Encke is approximately 10^5 years. We see evidence of a new "secular" behavior in P/Encke and some other comets that acts on a longer timescale and is of a different nature than the previously known averaged effects of Jupiter alone. This behavior may be associated with resonances with the planetary secular frequencies.

(6) Roughly 0.3% of SPCs spend some time in Earth-crossing orbits with $T > 3$ (non-Jupiter-crossing), i.e., become what are commonly called Near Earth Objects.

(7) The very flat initial inclination distribution of JFCs is observed to thicken as it ages. This is due to the inclination of individual comets increasing with time. For reasonable values of the physical fading time of comets (2000 to 10,000 years), we predict that there should be 5–20 times more extinct visible ($q < 2.5$ AU) JFCs than active visible JFCs. The extinct population is significantly less flattened than the active group, having a mean $\cos(i)$ of

0.88, consistent with the observations of a group of extinct JFCs by SS93.

(8) We show that the most likely explanation for the evolution in inclination is that the JFCs originate in a flattened distribution such as the Kuiper Belt.

(9) The evolution of the distribution in the argument of perihelion ω and the aphelion distance Q suggests that much of the current population of visible JFCs have relatively recently been scattered into a visible orbit ($q < 2.5$ AU) by Jupiter.

The (400 Megabyte) database from the simulations described here may be obtained by contacting the authors. In addition, a printed catalog is available which plots the evolution of the orbital elements of all the objects in the study.

APPENDIX A

In this appendix we develop the mechanics for interpreting the behavior of the inclination distribution seen in our integrations (see Section 3c). Using these integrations, it is possible to predict the number of extinct visible ($q \leq$ 2.5 AU) Jupiter-family comets (JFC) and their inclination distribution as functions of their physical lifetime.

Define τ as the age of a visible JFC. By this we mean the length of time since the comet was *first* injected into an orbit with $q \leq 2.5$ AU and $T \geq 2$. Define $\zeta(i, \tau)$ as the number of comets in the visible Jupiter-family with inclination i between i and $i + di$ and whose age is between τ and $\tau + d\tau$. If there were no physical aging and comets did not become extinct, then the observed inclination distribution would be

$$\xi(i; t = 0) = \int_0^\infty \zeta(i, \tau)d\tau. \qquad (A1)$$

Note that in the situation where comets do become extinct, $\xi(i; t = 0)$ is the current inclination distribution of both the active and extinct JFCs with $q \leq 2.5$ AU. If we model the effects of physical aging by *assuming* that all comets remain active for t_f years, after which they are permanently extinct, then the inclination distribution of the active visible JFCs is

$$\xi_{active}(i, t = 0) = \int_0^{t_f} \zeta(i, \tau)d\tau.$$

Our integrations follow the dynamical behavior of the known population of JFCs. Since we are not injecting any new comets into the system, at some time, t, we see the inclination distribution of the set of objects with ages between t and $t + t_f$. Therefore, the observed inclination distribution of objects in our integration is

$$\xi(i; t) = \int_t^{t+t_f} \zeta(i, \tau)d\tau.$$

Clearly, the observed inclination distribution of both active and extinct JFCs with $q \leq 2.5$ (Eq. (A1)) is

$$\xi(i; t = 0) = \int_0^\infty \zeta(i, \tau)d\tau$$

$$= \int_0^{t_f} \zeta(i, \tau)d\tau + \int_{t_f}^{2t_f} \zeta(i, \tau)d\tau + \cdots$$

$$+ \int_{nt_f}^{(n+1)t_f} \zeta(i, \tau)d\tau + \cdots$$

$$= \sum_{n=0}^\infty \xi(i; nt_f),$$

where $\xi(i; nt_f)$ can be determined for each n directly from our integrations. With a similar argument we find that the observed inclination distribution for the extinct comets is

$$\xi_{extinct}(i; t = 0) = \sum_{n=1}^\infty \xi(i; nt_f).$$

Note that the sum starts at 1 here, rather than at 0 as in the calculation of $\xi(i; t = 0)$. In this way, we can assume any value of t_f and perform the sums using the data stored from our integrations.

The total number of both active and extinct JFCs currently in the solar system is then

$$N_{tot} = \int_0^\tau \zeta_o(i; t = 0)di.$$

Also the mean cos(i) of the distribution of these comets is

$$\text{mean } \cos(i) = \frac{1}{N_{tot}} \int_0^\tau \zeta_o(i; t = 0) \cos(i)\, di.$$

Similar integrals exist for the population that only consists of extinct comets. It is these values that are discussed in Section 3c.

REFERENCES

BAILEY, M. E., J. F. CHAMBERS, AND G. HAHN 1992. Origin of Sungrazers: A frequent cometary end-state. *Astron. Astrophys.* **257**, 315.

BELYAEV, N. 1967. The orbit evolution of Comets Neujmin 2 (1916 II), Comas Solá (1927 III), Schwassman-Wachmann 2 (1929 I) for 400 years (1660–2060). *Astron. Zh.* **44**, 461.

CARUSI, A., L. KRESA'K, E. PEROZZI, AND G. VALSECCHI 1985. *Long-Term Evolution of Short-Period Comets,* Adam Hilger: Bristol.

CARUSI, A., AND G. VALSECCHI 1987. Dynamical evolution of short-period comets. In *Interplanetary Matter* (Z. Ceplecha and P. Pecina, Eds.), p. 21.

COHEN, C. J., E. C. HUBBARD, AND C. OSTERWINTER 1973. Elements of the outer planets for one million years. *Astron. Pap. Am. Ephem.* **22**, 3.

DANBY, J. M. A. 1988. *Fundamentals of Celestial Mechanics,* Willmann–Bell:Richmond.

DUNCAN, M., T. QUINN, AND S. TREMAINE 1988. The origin of short-period comets. *Astrophys. J.* **328**, L69.

EVERHART, E. 1972. The origin of short-period comets. *Astrophys. Lett.* **10**, 131.

EVERHART, E. 1985. An efficient integrator that uses Gauss-Radau spacing. In *Proceedings of IAU Colloquium No. 83: "Dynamics of Comets: Their Origin and Evolution"* (A. Carusi and G. Valsecchi Eds.), p. 185.

FERNÁNDEZ, J. 1980. On the existence of a comet belt beyond Neptune. *Mon. Not. Roy. Astron. Soc.* **192**, 481.

FERNÁNDEZ, J., H. RICKMAN, AND L. KAMÉL 1992. The population size and distribution of perihelion distances of the Jupiter family. To appear in *Proceedings of the International Workshop on Periodic Comets* (J. Fernández and H. Rickman, Eds.).

FOREST, E., AND R. D. RUTH 1990. Fourth-order symplectic integration. *Physica D* **43**, 105.

KARM, J., AND H. RICKMAN 1982. Pre-Discovery encounters between short-period comets and Jupiter estimated by Keplerian approximation. *Bull. Astron. Inst. Czechosl.* **33**, 359.

KAZIMIRCHAK-POLONSKAYA, E. 1967. Evolution des orbites des cométes á courte période au cours des années 1660–2060 et le rôle des planéts extérieures dans cette evolution, *Astron. Zh.* **44**, 439.

KRESÁK, L. 1981. Comet discoveries, statistics, and observational selection. In *Comets* (L. L. Wikening, Ed.), p. 56.

LEVISON, H. 1991. The state of knowledge concerning the Kuiper Belt. To appear in *Asteroids, Meteoroids, and Comets 1991* (A. Harris and E. Bowell, Eds.).

LINDGREN, M. 1991. Dynamical timescales in the Jupiter family. To appear in *Asteroids, Meteoroids, and Comets 1991* (A. Harris, and E. Bowell, Eds.).

LISSAUER, J. 1993. Planet formation. To appear in *Ann. Rev. Astron. Astrophys.* **31.**

MARSDEN, B. 1989. *Catalog of Cometary Orbits,* Smithsonian Astrophysical Observatory, Cambridge.

MORBIDELLI, A., AND J. HENRARD 1991. Secular resonances in the asteroid belt: Theoretical perturbation approach and the problem of their location. *Celestial Mech. Dynam. Astron.* **51**, 131.

MURRAY, C. D., AND K. FOX 1984. Structure of the 3 : 1 jovian resonance: A comparison of numerical methods. *Icarus* **59**, 221.

NAKAMURA, T., AND M. YOSHIKAWA 1991. COSMO-DICE: Dynamical investigation of cometary evolution. *Publ. Natl. Astron. Obs. Jpn.* **2**, 293.

NEWTON, H. 1893. On the capture of comets by planets, especially their capture by Jupiter. *Mem. Natl. Acad. Sci.* **6**, 7.

OLSSON-STEEL, D. 1988. Meteoroid streams and the Zodiacal dust cloud. In *Catastrophes and Evolution: Astronomical Foundations* (S. Clube, Ed.), p. 169.

ÖPIK, E. 1963. The stray bodies in the Solar System. Part 1. Survival of cometary nuclei and asteroids. *Adv. Astron. Astrophys.* **2**, 219.

QUINN, T., S. TREMAINE AND M. DUNCAN 1990. Planetary perturbations and the origin of short-period comets. *Astrophys. J.* **355**, 667.

RICKMAN, H. 1991. Physico-dynamical evolution of aging comets. To appear in *Proceedings of the 1991 Goutelas Spring School of Astrophysics: Interrelations entre la Physique et la Dynamique des Petits Corps du Systéme Solaire.*

SAHA, P., AND S. TREMAINE 1993. Sympletic integrators for Solar System dynamics. *Astron. J.* **104**, 1633.

SHOEMAKER, E. M., AND C. S. SHOEMAKER 1993. Active and extinct earth-crossing periodic comets. To be submitted.

SHOEMAKER, E., AND R. WOLFE 1982. Cratering time scales for the Galilean satellites. In *Satellites of Jupiter* (D. Marrison, Ed.), p. 277.

STAGG, C., AND M. BAILEY 1989. Stochastic capture of short-period comets. *Mon. Not. Roy. Astron. Soc.* **241**, 507.

STIEFEL, E. L., AND G. SCHIEFELE 1971. *Linear and Regular Celestial Mechanics,* Springer-Verlag, New York.

STOER, J., AND R. BULIRSCH 1980. Introduction to numerical analysis. Springer-Verlag, New York.

TANCREDI, G., M. LINDGREN, AND H. RICKMAN 1990. Temporary satellite capture and orbital evolution of Comet P/Helin–Roman–Crockett. *Astron. Astrophys.* **239**, 375.

TANCREDI, G., AND M. LINDGREN 1992. The vicinity of Jupiter: A region to look for comets. To appear in *Asteroids, Meteoroids, and Comets 1991* (A. Harris and E. Bowell, Eds.).

TANCREDI, G., AND H. RICKMAN 1992. The evolution of Jupiter family comets over 2000 years. In *Chaos, Resonance and Collective Dynamical Phenomena in the Solar System* (S. Ferraz-Mello, Ed.), p. 269.

WEISSMAN, P. R., M. F. A'HEARN, L. A. MCFADDEN, AND H. RICKMAN 1989. Evolution of comets into asteroids. In *Asteroids II* (R. P. Binzel, T. Gehrels, and M. S. Matthews, Eds.), p. 880.

WETHERILL, G. 1991. End products of cometary evolution: Cometary origin of earth-crossing bodies of asteroidal appearance. In *Comets in the post-Halley era* (R. L. Newburn, M. Neugebauer, and J. Rahe, Eds.), p. 537.

WISDOM, J., AND M. HOLMAN 1991. Symplectic maps for the N-body problem. *Astron. J.* **102**, 1528.

YOSHIDA, H. 1990. Construction of higher order symplectic integrators. *Phys. Lett. A* **150**, 262.